

Study of the $B^- \rightarrow \Lambda_c^+ \bar{\Lambda}_c^- K^-$ decay

R. Aaij *et al.*^{*}
(LHCb Collaboration)

 (Received 3 November 2022; accepted 5 January 2023; published 27 July 2023)

The decay $B^- \rightarrow \Lambda_c^+ \bar{\Lambda}_c^- K^-$ is studied in proton-proton collisions at a center-of-mass energy of $\sqrt{s} = 13$ TeV using data corresponding to an integrated luminosity of 5 fb^{-1} collected by the LHCb experiment. In the $\Lambda_c^+ K^-$ system, the $\Xi_c(2930)^0$ state observed at the *BABAR* and Belle experiments is resolved into two narrower states, $\Xi_c(2923)^0$ and $\Xi_c(2939)^0$, whose masses and widths are measured to be $m(\Xi_c(2923)^0) = 2924.5 \pm 0.4 \pm 1.1$ MeV, $m(\Xi_c(2939)^0) = 2938.5 \pm 0.9 \pm 2.3$ MeV, $\Gamma(\Xi_c(2923)^0) = 4.8 \pm 0.9 \pm 1.5$ MeV, $\Gamma(\Xi_c(2939)^0) = 11.0 \pm 1.9 \pm 7.5$ MeV, where the first uncertainties are statistical and the second systematic. The results are consistent with a previous LHCb measurement using a prompt $\Lambda_c^+ K^-$ sample. Evidence of a new $\Xi_c(2880)^0$ state is found with a local significance of 3.8σ , whose mass and width are measured to be $2881.8 \pm 3.1 \pm 8.5$ MeV and $12.4 \pm 5.3 \pm 5.8$ MeV, respectively. In addition, evidence of a new decay mode $\Xi_c(2790)^0 \rightarrow \Lambda_c^+ K^-$ is found with a significance of 3.7σ . The relative branching fraction of $B^- \rightarrow \Lambda_c^+ \bar{\Lambda}_c^- K^-$ with respect to the $B^- \rightarrow D^+ D^- K^-$ decay is measured to be $2.36 \pm 0.11 \pm 0.22 \pm 0.25$, where the first uncertainty is statistical, the second systematic and the third originates from the branching fractions of charm hadron decays.

DOI: [10.1103/PhysRevD.108.012020](https://doi.org/10.1103/PhysRevD.108.012020)

I. INTRODUCTION

The quark model predicts a rich spectrum of singly charmed baryons. However, many states, especially those containing at least one s quark (e.g. Ξ_c^0, Ω_c^0), have not been experimentally established. An effective approach to search for charm baryons is in b -hadron decays. Upon the observation of the $B^- \rightarrow \Lambda_c^+ \bar{\Lambda}_c^- K^-$ decay,¹ the *BABAR* collaboration reported evidence of a $\Xi_c(2930)^0$ state in the $\Lambda_c^+ K^-$ system with a low significance [1]; and later the Belle collaboration confirmed this with a larger yield [2]. Recently, the Belle collaboration also found evidence of its charged counterpart in the $B^0 \rightarrow \Lambda_c^+ \bar{\Lambda}_c^- K_S^0$ decay [3]. The LHCb experiment, with a much higher B meson yield and excellent momentum resolution, should be able to confirm the $\Xi_c(2930)^0$ state by examining the $B^- \rightarrow \Lambda_c^+ \bar{\Lambda}_c^- K^-$ decay, precisely measure its properties and resolve a potential finer structure.

Another way to look for charmed baryons is to search for their production in primary pp interactions, recently exploited by the LHCb experiment [4–7]. A search for excited Ξ_c^0 baryons in prompt $\Lambda_c^+ K^-$ pairs performed at the

LHCb experiment found that there are two narrow states, $\Xi_c(2923)^0$ and $\Xi_c(2939)^0$, at the position of $\Xi_c(2930)^0$ observed at B factories, with the presence of an additional $\Xi_c(2965)^0$ structure at higher mass [7]. At lower mass, a peaking structure is seen at around 2880 MeV,² noted as $\Xi_c(2880)^0$, which is obscured by partially reconstructed background but is in the position of an expected resonance [8]. The complexity of the current experimental situation motivates the study of the $B^- \rightarrow \Lambda_c^+ \bar{\Lambda}_c^- K^-$ decay at the LHCb experiment. Although the exclusive reactions have lower yield compared to the prompt search, the background level is expected to be lower.

Furthermore, the $B^- \rightarrow \Lambda_c^+ \bar{\Lambda}_c^- K^-$ decay provides a unique opportunity to search for possible exotic candidates in the $\Lambda_c^+ \bar{\Lambda}_c^-$ and $\bar{\Lambda}_c^- K^-$ spectra. The Belle collaboration observed a significant near-threshold enhancement in the $\Lambda_c^+ \bar{\Lambda}_c^-$ mass spectrum through the reaction $e^+e^- \rightarrow \Lambda_c^+ \bar{\Lambda}_c^- \gamma_{\text{ISR}}$, where γ_{ISR} indicates a high momentum photon emitted in the initial state radiation process [9]. The BESIII experiment recently measured the $e^+e^- \rightarrow \Lambda_c^+ \bar{\Lambda}_c^-$ cross-section with high precision, and an enhanced value near threshold was reported [10]. If the enhancement of the $\Lambda_c^+ \bar{\Lambda}_c^-$ production around 4600 MeV is due to the presence of a resonance, it might be confirmed in a decay of the type $B^- \rightarrow \Lambda_c^+ \bar{\Lambda}_c^- K^-$, despite the different production mechanism. The $\bar{\Lambda}_c^- K^-$ system does not form resonances in the conventional quark model.

^{*}Full author list given at the end of the article.

¹The inclusion of charge-conjugate processes is implied throughout the paper.

Published by the American Physical Society under the terms of the [Creative Commons Attribution 4.0 International license](https://creativecommons.org/licenses/by/4.0/). Further distribution of this work must maintain attribution to the author(s) and the published article's title, journal citation, and DOI. Funded by SCOAP³.

²Natural units with $\hbar = c = 1$ are used throughout this paper.

In this paper, a data sample of proton-proton (pp) collisions at $\sqrt{s} = 13$ TeV, corresponding to an integrated luminosity of 5 fb^{-1} , collected by the LHCb experiment in years of 2016 to 2018, is used to study the decay of $B^- \rightarrow \Lambda_c^+ \bar{\Lambda}_c^- K^-$. The Λ_c^+ baryon is reconstructed in the $pK^-\pi^+$ final state. The $B^- \rightarrow D^+ D^- K^-$ decay, with $D^+ \rightarrow K^-\pi^+\pi^+$, is chosen as the normalisation channel, since it has a very similar decay topology and the same number of tracks in the final state as the signal. This allows a precise measurement of the ratio of the branching fractions of the $B^- \rightarrow \Lambda_c^+ \bar{\Lambda}_c^- K^-$ and $B^- \rightarrow D^+ D^- K^-$ decays.

II. DETECTOR AND SIGNAL SELECTION

The LHCb detector [11,12] is a single-arm forward spectrometer covering the pseudorapidity range $2 < \eta < 5$, designed for the study of particles containing b or c quarks. The detector includes a high-precision tracking system consisting of a silicon-strip vertex detector (VELO) surrounding the pp interaction region, a large-area silicon-strip detector located upstream of a dipole magnet with a bending power of about 4 Tm, and three stations of silicon-strip detectors and straw drift tubes placed downstream of the magnet. The tracking system provides a measurement of the momentum, p , of charged particles with a relative uncertainty that varies from 0.5% at low momentum to 1.0% at 200 GeV. The minimum distance of a track to a primary pp collision vertex (PV), the impact parameter (IP), is measured with a resolution of $(15 + 29/p_T) \mu\text{m}$, where p_T is the component of the momentum transverse to the beam, in GeV. The momentum scale is calibrated using samples of $J/\psi \rightarrow \mu^+\mu^-$ and $B^- \rightarrow J/\psi K^+$ decays collected concurrently with the data sample used for this analysis [13,14]. Different types of charged hadrons are distinguished using information from two ring-imaging Cherenkov detectors. Photons, electrons and hadrons are identified by a calorimeter system consisting of scintillating-pad and preshower detectors, an electromagnetic and a hadronic calorimeter. Muons are identified by a system composed of alternating layers of iron and multiwire proportional chambers. The online event selection is performed by a trigger, which consists of a hardware stage, based on information from the calorimeter and muon systems, followed by a software stage, which applies a full event reconstruction. At the hardware trigger stage, events are required to have a muon with high p_T or a hadron, photon or electron with high transverse energy in the calorimeters. The software trigger requires a two-, three- or four-track secondary vertex with a significant displacement from any primary pp interaction vertex. Simulation is required to model the effects of the detector acceptance and the imposed selection requirements. In the simulation, pp collisions are generated using PYTHIA 8 [15] with a specific LHCb configuration [16]. Decays of unstable particles are described by EvtGen [17], in which final-state radiation is generated using PHOTOS [18]. The interaction of the generated particles with the detector, and its response, are implemented using the Geant4 toolkit [19] as described in Ref. [20].

The B^- candidates are reconstructed with a pair of $\Lambda_c^+ \bar{\Lambda}_c^-$ baryons along with a companion kaon, where the Λ_c^+ baryon is reconstructed in the $\Lambda_c^+ \rightarrow pK^-\pi^+$ final state. The Λ_c^+ decay products are required to have good track quality and large transverse momentum, to be inconsistent with originating from any PV, and to have correct particle identification (PID) (proton, kaon or pion). The Λ_c^+ candidate is required to have p_T greater than 1.8 GeV, its vertex inconsistent with originating from any PV, and the angle between its momentum and its flight direction with respect to the associated PV to be less than 90 degrees. In case of multiple primary vertices, the candidate is associated to the PV with respect to which the smallest χ_{IP}^2 is obtained, where χ_{IP}^2 is defined as the difference in the vertex-fit χ^2 of the associated PV reconstructed with and without the track under consideration. The reconstructed mass of the Λ_c^+ candidates is required to be within the window of $2225 < M(pK^-\pi^+) < 2345$ MeV. Higher thresholds on p_T and momentum are set for the companion kaon and similar requirements as for the Λ_c^+ decay products are imposed on its track quality, PID and displacement from the PV. All the selection criteria for the Λ_c^+ candidates apply to the $\bar{\Lambda}_c^-$ candidates. The B^- candidates are required to have p_T greater than 5 GeV, a reconstructed lifetime longer than 0.2 ps, and to have a χ_{IP}^2 less than 25. The reconstructed B^- flight direction, defined by its production and decay vertices, and its momentum are required to be well aligned. The B^- candidate must be within the mass window of $5205 < M(\Lambda_c^+ \bar{\Lambda}_c^- K^-) < 5355$ MeV.

To further suppress the background, a boosted decision tree (BDT) [21,22], implemented in the TMVA toolkit [23], is trained with the simulated sample as signal and with data from sideband regions defined in Table I as background. The training variables are the χ^2 per degree of freedom of the Λ_c^+ decay vertex, and the χ_{IP}^2 and PID information of all final-state tracks. The PID values in simulation are drawn from calibration samples to better agree with real data [24]. The selection requirement on the BDT output is chosen to optimise the expected significance of the $B^- \rightarrow \Lambda_c^+ \bar{\Lambda}_c^- K^-$ signal.

A dedicated BDT is trained for the normalization channel $B^- \rightarrow D^+ D^- K^-$ with simulation as signal and with candidates in the D^+ and B^- sideband regions, as defined in Table I, as the proxy for background. The signal region of the $B^- \rightarrow D^+ D^- K^-$ decay is wider than the $B^- \rightarrow \Lambda_c^+ \bar{\Lambda}_c^- K^-$ since the energy release (Q -value) of the former is larger. The

TABLE I. Definitions of the sideband regions, where $m(B^-)$ and $m(D^+)$ represent the known values from Ref. [25]. The same sideband region is defined for the $\bar{p}K^+\pi^-$ combination as for the $pK^-\pi^+$ combination. The values are in MeV.

	$50 < M(\Lambda_c^+ \bar{\Lambda}_c^- K^-) - m(B^-) < 90$ MeV,
$B^- \rightarrow \Lambda_c^+ \bar{\Lambda}_c^- K^-$	$2225 < M(pK^-\pi^+) < 2260$ MeV or $2310 < M(pK^-\pi^+) < 2345$ MeV
$B^- \rightarrow D^+ D^- K^-$	$75 < M(D^+ D^- K^-) - m(B^-) < 120$ MeV, $45 < M(K^-\pi^+\pi^+) - m(D^+) < 90$ MeV

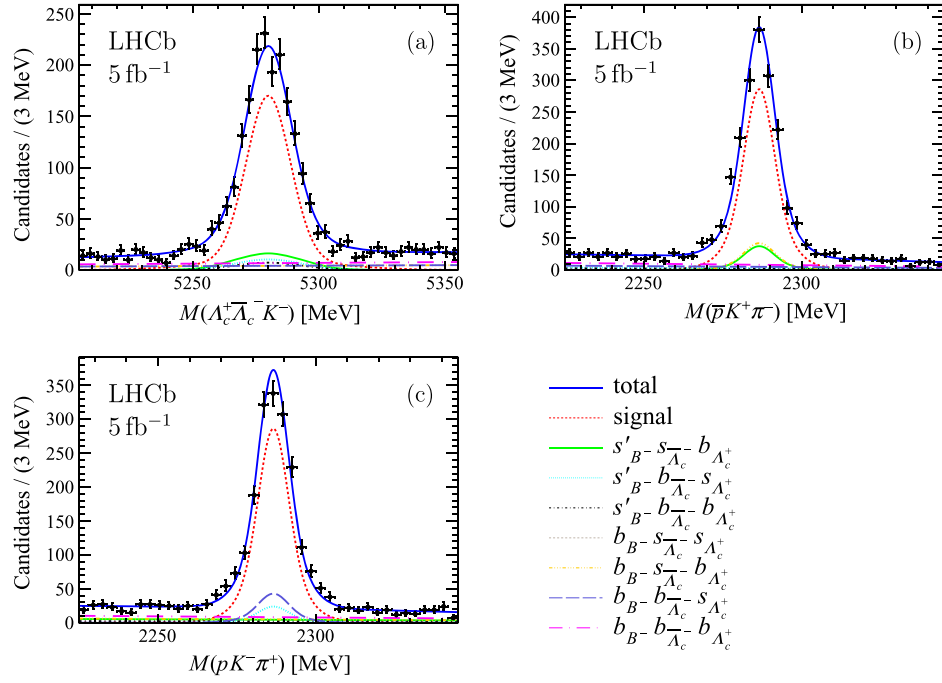


FIG. 1. Distributions of (a) $M(\Lambda_c^+ \bar{\Lambda}_c^- K^-)$, (b) $M(\bar{p} K^+ \pi^-)$ and (c) $M(p K^- \pi^+)$ of selected $B^- \rightarrow \Lambda_c^+ \bar{\Lambda}_c^- K^-$ candidates. The data points with error bars are shown along with the total fitted shape, which is composed of signal and background components, as shown in the legend.

selection is almost identical to the signal selection, with the Λ_c^+ candidate replaced by the D^+ reconstructed from the $K^- \pi^+ \pi^+$ decay mode. The D^+ candidates are required to be within a mass window of $1795 < M(K^- \pi^+ \pi^+) < 1945$ MeV.

III. SIGNAL EXTRACTION

The $B^- \rightarrow \Lambda_c^+ \bar{\Lambda}_c^- K^-$ signal is extracted using a three-dimensional (3D) fit to the invariant mass of B^- , Λ_c^+ and $\bar{\Lambda}_c^-$ candidates. The 3D fit function is constructed as a sum of multiple terms each of which is a direct product of one-dimensional functions. The signal function is $s_{B^-} s_{\bar{\Lambda}_c^-} s_{\Lambda_c^+}$, where s_{B^-} is modeled by sum of two Gaussian functions sharing common mean value and $s_{\Lambda_c^+}$ is modelled using sum of three Gaussian functions with a common mean value fixed to the known Λ_c^+ mass [25]. The fit model and parameters are identical for $s_{\Lambda_c^+}$ and $s_{\bar{\Lambda}_c^-}$. The Gaussian parameters are all fixed to values from fits to simulated samples. The background shape in the $M(\Lambda_c^+ \bar{\Lambda}_c^- K^-)$ and $M(p K^- \pi^+)$ distributions is parameterised with a first-order polynomial. The background candidates are of seven different categories: from real B^- decay products, (1) $s'_{B^-} s_{\bar{\Lambda}_c^-} b_{\Lambda_c^+}$, (2) $s'_{B^-} b_{\bar{\Lambda}_c^-} s_{\Lambda_c^+}$, (3) $s'_{B^-} b_{\bar{\Lambda}_c^-} b_{\Lambda_c^+}$; from non- B^- decays containing true Λ_c decays, (4) $b_{B^-} s_{\bar{\Lambda}_c^-} s_{\Lambda_c^+}$, (5) $b_{B^-} s_{\bar{\Lambda}_c^-} b_{\Lambda_c^+}$, (6) $b_{B^-} b_{\bar{\Lambda}_c^-} s_{\Lambda_c^+}$; and pure combinatorial background, (7) $b_{B^-} b_{\bar{\Lambda}_c^-} b_{\Lambda_c^+}$. For background categories (1)–(3) the Q -values of B^- decays could differ from the signal, and a single Gaussian s'_{B^-} is used. The fitted B^- , Λ_c^+ and $\bar{\Lambda}_c^-$ mass spectra are shown in Fig. 1. The signal yield is determined to be 1365 ± 42 . It is found that background (4) $b_{B^-} s_{\bar{\Lambda}_c^-} s_{\Lambda_c^+}$ makes negligible contribution; thus the yield is fixed to zero.

The resonance structure present in the $B^- \rightarrow \Lambda_c^+ \bar{\Lambda}_c^- K^-$ decay is studied using the candidates in narrower B^- and Λ_c^+ mass windows: $5240 < M(\Lambda_c^+ \bar{\Lambda}_c^- K^-) < 5320$ MeV and $2265 < M(p K^- \pi^+) < 2305$ MeV, respectively. In order to improve the mass resolution of any resonant state, a refit of the decay fixing the masses of Λ_c^+ and B^- to the known values is performed. The refitted momenta of Λ_c^+ , $\bar{\Lambda}_c^-$ and K^- are used to determine the $M(\Lambda_c^+ K^-)$, $M(\bar{\Lambda}_c^- K^-)$ and $M(\Lambda_c^+ \bar{\Lambda}_c^-)$ mass spectra. It is verified that the selection requirements do not induce artificial peaking structures. For background subtraction, it is sufficient to consider the sideband in the two-dimensional spectrum of $M(p K^- \pi^+)$ and $M(\bar{p} K^+ \pi^-)$, as shown in Fig. 2, since the absence of

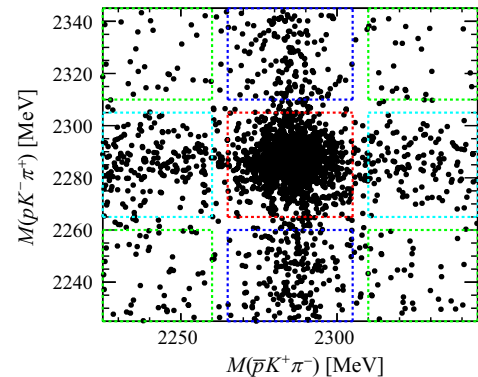


FIG. 2. Selected $B^- \rightarrow \Lambda_c^+ \bar{\Lambda}_c^- K^-$ candidates in the two-dimensional $M(p K^- \pi^+)$ and $M(\bar{p} K^+ \pi^-)$ spectrum. The red dashed box is the signal region, the dark blue, light blue and green boxes indicate regions dominated by $s_{\bar{\Lambda}_c^-} b_{\Lambda_c^+}$, $b_{\bar{\Lambda}_c^-} s_{\Lambda_c^+}$ and combinatorial background, respectively.

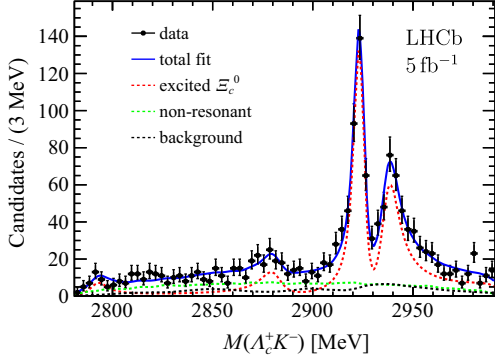


FIG. 3. Mass spectrum of the $\Lambda_c^+ K^-$ pair from the $B^- \rightarrow \Lambda_c^+ \bar{\Lambda}_c^- K^-$ decays. The data points with error bars are shown along with the total fitted shape in blue solid line, which is composed of the components, as shown in the legend.

the $b_{B^-} s_{\bar{\Lambda}_c^-} s_{\Lambda_c^+}$ background component means that whenever a true $\Lambda_c^+ \bar{\Lambda}_c^-$ pair is selected, it corresponds to a real $B^- \rightarrow \Lambda_c^+ \bar{\Lambda}_c^- K^-$ decay. The contributions from $s_{\bar{\Lambda}_c^-} b_{\Lambda_c^+}$ and $b_{\bar{\Lambda}_c^-} s_{\Lambda_c^+}$ are averaged to account for the background contribution in the signal region, where the double-counted contribution from pure combinatorial background, as in $b_{\bar{\Lambda}_c^-} b_{\Lambda_c^+}$, is subtracted. The background subtraction is also performed with the *sPlot* method [26] as a cross-check to verify that none of the observed structures are due to background fluctuations.

The $M(\Lambda_c^+ K^-)$ spectrum is shown in Fig. 3. The fitting function is described in detail in Sec. IV. Two states reported in Ref. [7], $\Xi_c(2923)^0$ and $\Xi_c(2939)^0$, are

observed. In addition, a wide structure is evident around 2880 MeV. A similar structure was observed in the prompt $\Lambda_c^+ K^-$ study [7], but background due to feed-down from higher Ξ_c^0 states, $\Xi_c(3055)^0$ and $\Xi_c(3080)^0$, with a π^0 or π^+ missing in the reconstruction, could not be discounted. Such background will not affect the $\Lambda_c^+ K^-$ system from B^- decays, since there is not enough phase space for $B^- \rightarrow \bar{\Lambda}_c^- \Xi_c(3055/3080)^0$ and such feed-down component with a missing particle will not peak at the B^- mass. To study the effect of partially reconstructed $\Xi_c(3055/3080)^0$ from other b -hadron decays, a sample of Λ_b^0 decays is generated with the decay chain $\Lambda_b^0 \rightarrow \Xi_c(3055)^+ D^-$, $\Xi_c(3055)^+ \rightarrow [\Lambda_c^+ \pi^+]_{\Sigma_c^+} K^-$, $D^- \rightarrow K^+ \pi^- \pi^-$. The selection criteria remove them completely. Therefore, the wide structure cannot be due to feed-down, and is considered as a resonant state in the fit. Both $\Xi_c(2790)^0$ and $\Xi_c(2815)^0$ states are expected at the lower end of the $M(\Lambda_c^+ K^-)$ spectrum, and their masses, widths and spin-parity J^P are fixed to known values [25]. The $\Xi_c(2790)^0$ state has $J^P = (1/2)^-$ and $\Xi_c(2815)^0$ has $J^P = (3/2)^-$. However, the significance of the $\Xi_c(2815)^0$ state is only 2.1σ , and so it is not included in the nominal fit. The yield of the resonant states is not enough to determine their quantum numbers with sufficient significance. The spin-parity J^P of both $\Xi_c(2923)^0$ and $\Xi_c(2939)^0$ states is fixed to be $(3/2)^-$ and that of $\Xi_c(2880)^0$ is fixed to $(1/2)^-$ [8].

The invariant mass distributions of the $\bar{\Lambda}_c^- K^-$ and $\Lambda_c^+ \bar{\Lambda}_c^-$ pairs are shown in Fig. 4. No significant structure is

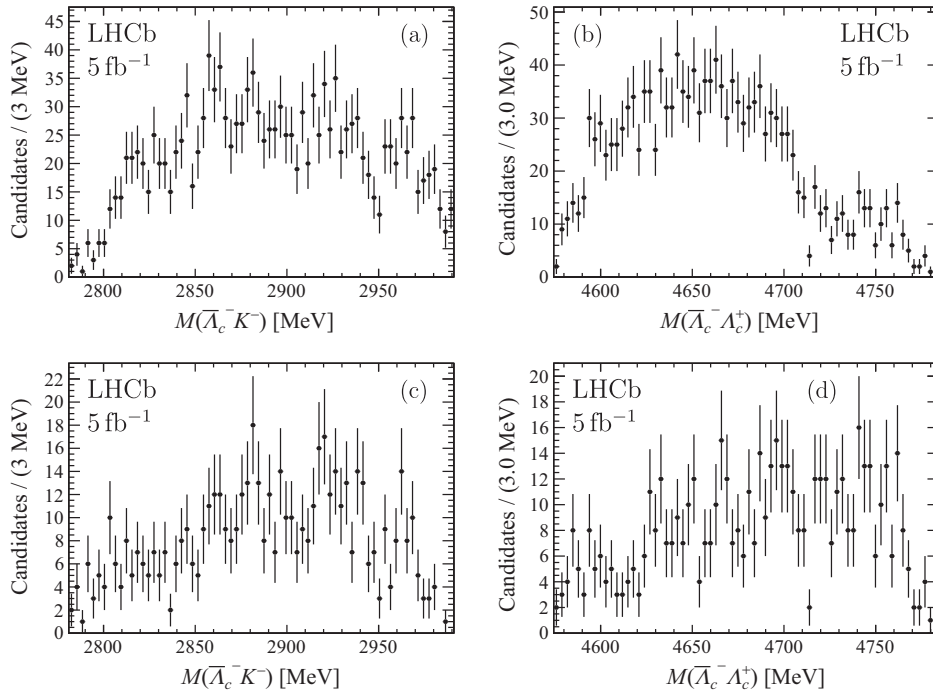


FIG. 4. Mass spectrum of (a),(c) $\bar{\Lambda}_c^- K^-$ and (b),(d) $\Lambda_c^+ \bar{\Lambda}_c^-$ pairs from (a),(b) all the $B^- \rightarrow \Lambda_c^+ \bar{\Lambda}_c^- K^-$ candidates and (c),(d) after vetoing candidates with $2900 < M(\Lambda_c^+ K^-) < 2970$ MeV.

seen. The distributions of $M(\bar{\Lambda}_c^- K^-)$ and $M(\Lambda_c^+ \bar{\Lambda}_c^-)$ are also produced after rejecting candidates with $2900 < M(\Lambda_c^+ K^-) < 2970$ MeV, to remove contributions from the $\Xi_c(2923)^0$ and $\Xi_c(2939)^0$ states. No significant structure is seen.

IV. MASSES AND WIDTHS OF THE EXCITED Ξ_c^0 STATES

The masses and widths of the excited Ξ_c^0 states are obtained from an unbinned maximum likelihood fit to the $M(\Lambda_c^+ K^-)$ spectrum. The total fitting function is constructed as

$$f(M) = \frac{N_{\Xi_c^0}}{N_{\text{evt}}} f_{\Xi_c^0}(M) \otimes g(\sigma_{\text{res}}) + \frac{N_{\text{phsp}}}{N_{\text{evt}}} f_{\text{phsp}}(M) + \frac{N_{\text{bkg}}}{N_{\text{evt}}} f_{\text{bkg}}(M), \quad (1)$$

where M stands for $M(\Lambda_c^+ K^-)$. The function describing the excited Ξ_c^0 states, $f_{\Xi_c^0}$, which will be discussed in detail later, is convolved with a Gaussian function to account for the detector resolution. The Gaussian function has a mean value of zero and width σ_{res} in the range of 0–2 MeV dependent on $M(\Lambda_c^+ K^-)$. The resolution σ_{res} is parameterised as $(M - m_{\text{lo}})^a (m_{\text{up}} - M)^b [c + d(M - m_{\text{lo}})]$, where $m_{\text{lo}} = m(\Lambda_c^+) + m(K^-)$ and $m_{\text{up}} = m(B^-) - m(\bar{\Lambda}_c^-)$ are lower and upper thresholds of the $M(\Lambda_c^+ K^-)$ spectrum, respectively, and a, b, c, d are determined from simulation. The contribution from the non-resonant component f_{phsp} is modeled with simulation of pure phase-space decay. The background contribution f_{bkg} is extrapolated from the sideband regions as defined in Fig. 2. The expected number of background events N_{bkg} is also fixed using extrapolation from the sideband regions. The total number of candidates within the fitting range, N_{evt} , is 1494. All fitting functions are normalised to unity.

As discussed in Sec. III, four excited states are considered: $\Xi_c(2790)^0$, $\Xi_c(2880)^0$, $\Xi_c(2923)^0$ and $\Xi_c(2939)^0$. The interference between the $\Xi_c(2923)^0$ and $\Xi_c(2939)^0$ states is important and cannot be neglected to correctly describe the data. The significance of the two-state hypothesis with respect to the hypothesis of a single $\Xi_c(2930)^0$ state is over 11σ . The function used for excited Ξ_c^0 states is expressed as

$$f_{\Xi_c^0} = pq(|\mathcal{M}_{\Xi_c(2790)^0} + \mathcal{M}_{\Xi_c(2880)^0}|^2 + |\mathcal{M}_{\Xi_c(2923)^0} + \mathcal{M}_{\Xi_c(2939)^0}|^2), \quad (2)$$

where $\mathcal{M}_\alpha(M) = \hat{A}_\alpha(M) F_{l_\alpha}(q) F_{L_\alpha}(p)$. The quantities q and p represent the breakup momenta of the Ξ_c^0 and B^- decays, expressed as $q = \lambda^{1/2}(M^2, m_K^2, m_{\Lambda_c}^2)/(2M)$, $p = \lambda^{1/2}(m_B^2, M^2, m_{\Lambda_c}^2)/(2M)$, where $\lambda(x, y, z) = x^2 + y^2 +$

$z^2 - 2xy - 2yz - 2zx$. The subscript α runs through all four resonant states considered in the fit. The amplitude of each state is described by a relativistic Breit–Wigner function,

$$\hat{A}_\alpha(M) = \frac{c_\alpha}{m_\alpha^2 - M^2 - im_\alpha \Gamma_\alpha \frac{q}{q_\alpha} \cdot \frac{m_\alpha}{M} \cdot \frac{F_{l_\alpha}(q)^2}{F_{l_\alpha}(q_\alpha)^2}}, \quad (3)$$

where m_α and Γ_α are the mass and width of the state, c_α is a complex coefficient, and q_α is the breakup momentum q computed at the mass m_α . The quantities $F_l(q)$ and $F_L(p)$ are Blatt–Weisskopf barrier functions, defined as

$$F_k(q) = \begin{cases} 1 & k = 0, \\ \sqrt{\frac{(qr)^2}{1+(qr)^2}} & k = 1, \\ \sqrt{\frac{(qr)^4}{9+3(qr)^2+(qr)^4}} & k = 2, \end{cases} \quad (4)$$

where r is the effective radius of the resonant state, fixed to 3.0 GeV^{-1} [27], l is the orbital angular momentum between the $\bar{\Lambda}_c^-$ and K^+ particles, and L is the smallest possible orbital angular momentum between the Λ_c^+ and Ξ_c^0 states. As mentioned before, the spin-parity of the $\Xi_c(2790)^0$ state is known to be $(1/2)^-$ [25]. The 1P multiplet contains 5 states with the quantum numbers $(1/2)^-$, $(1/2)^-$, $(3/2)^-$, $(3/2)^-$ and $(5/2)^-$. The quantum numbers of the $\Xi_c(2880)^0$ state are assumed to be $(1/2)^-$ as well [8]. The spin-parity of the $\Xi_c(2923)^0$ and $\Xi_c(2939)^0$ states is assumed to be $(3/2)^-$. The values of l are set to respect momentum and parity conservation, namely $l = 0$ for the $\Xi_c(2790)^0$ and $\Xi_c(2880)^0$ states and $l = 2$ for the $\Xi_c(2923)^0$ and $\Xi_c(2939)^0$ states. Alternative assumptions for the quantum numbers of the states are considered in the determination of the systematic uncertainty. If the spin of the Ξ_c^0 of interest is J , then L can only take values $J - 1/2$ and $J + 1/2$, and F_{L_α} is replaced by $F_{J_\alpha-1/2} + k_\alpha F_{J_\alpha+1/2}$. The k_α parameters are complex factors representing the contribution of the higher partial waves. They cannot be extracted from a one-dimensional fit with the available statistics, and all k_α parameters are set to a common value of k_0 in the fit.

To study the possible bias on the measured mass and width of the $\Xi_c(2923)^0$ and $\Xi_c(2939)^0$ states, 3 000 pseudoexperiments are performed where all other parameters, except the masses and widths, are fixed. A fit is performed for each pseudoexperiment, and the pull of each mass or width parameter is calculated with respect to the input. The pull is defined as the difference between the fitted value and the input value, divided by the uncertainty obtained from the fit. The pull distributions are then fitted with Gaussian functions. The deviation of the Gaussian mean from zero is used to correct the fitted mass values. The correction values are smaller than the statistical uncertainties and will be considered in the systematic uncertainty determination.

TABLE II. Measured masses, widths and significance of excited Ξ_c^0 states.

State	Mass (MeV)	Width (MeV)	Significance
$\Xi_c(2880)^0$	$2881.8 \pm 3.1 \pm 8.5$	$12.4 \pm 5.2 \pm 5.8$	3.8σ
$\Xi_c(2923)^0$	$2924.5 \pm 0.4 \pm 1.1$	$4.8 \pm 0.9 \pm 1.5$	$> 10\sigma$
$\Xi_c(2939)^0$	$2938.5 \pm 0.9 \pm 2.3$	$11.0 \pm 1.9 \pm 7.5$	$> 10\sigma$

The fitted $M(\Lambda_c^+ K^-)$ distribution is shown in Fig. 3, and the measured masses and widths are listed in Table II. The significance of the $\Xi_c(2790)^0$ and $\Xi_c(2880)^0$ states is calculated by studying 30000 pseudoexperiments. Each is generated with a null hypothesis, then fitted both with and without the excited Ξ_c^0 state of interest. The test statistic t_0 , defined as twice the difference in log-likelihood with and without the state, $2 \log(\mathcal{L}_1/\mathcal{L}_0)$, is expected to follow a χ^2 distribution. The t_0 values from the pseudoexperiments are fitted with a χ^2 distribution, and the p -value of the observed yield corresponds to the fraction of integrated area above the t_0 value measured in real data divided by the total integrated area. The significance of both the $\Xi_c(2790)^0$ and $\Xi_c(2880)^0$ states is estimated to be 3.9σ . The significance of the $\Xi_c(2880)^0$ state is stable even assuming the absence of the $\Xi_c(2790)^0$ state.

Systematic uncertainties on the mass and width measurements from various sources are studied. Multiple alternative assumptions on the fixed parameters are tested. The spin-parity of the $\Xi_c(2923)^0$ and $\Xi_c(2939)^0$ states is set to $(1/2)^-$, $(1/2)^+$ or $(3/2)^-$, and J^P of the $\Xi_c(2880)^0$ is set to $(1/2)^+$, $(3/2)^-$ or $(3/2)^+$. In these tests, the states with the same spin-parity are always added coherently. The effective radius r is set to either 2.0 or 4.0 GeV $^{-1}$. The mass and width of the $\Xi_c(2790)^0$ state are varied within their uncertainty, and the hypothesis without the $\Xi_c(2790)^0$ state is tested. A different coefficient k_α is assigned to each group of Ξ_c^0 states with the same spin-parity. An additional state around 2970 MeV with orbital angular momentum of 0, 1 or 2 is added. The fit including the $\Xi_c(2815)^0$ state is considered. The potential interference with nonresonant decays is considered by adding a constant term in the $\Lambda_c^+ K^-$ mass distribution. The maximum variation in the fit results is obtained for each alternative assumption if multiple values are considered, and the total systematic uncertainty due to model assumptions is the quadratic sum of variation in all alternative assumptions.

The $\Xi_c(2923)^0$ and $\Xi_c(2939)^0$ lineshape is described alternatively using a K-matrix formalism [28], which preserves unitarity. The variation in the results is considered as a systematic uncertainty. The pull distributions from pseudoexperiments are used to correct a possible bias in the masses and widths of the $\Xi_c(2923)^0$ and $\Xi_c(2939)^0$ states, where the resulting corrections are smaller than statistical uncertainties. It is found that the fitted width σ_{pull} of the pull distribution is slightly wider than unity, indicating a

TABLE III. Systematic uncertainties on the masses and widths of the $\Xi_c(2923)^0$, $\Xi_c(2939)^0$ and $\Xi_c(2880)^0$ states. Values are given in MeV.

Source	$\Xi_c(2923)^0$		$\Xi_c(2939)^0$		$\Xi_c(2880)^0$	
	Mass	Width	Mass	Width	Mass	Width
Model assumption	0.8	1.4	1.9	7.0	8.4	4.1
Lineshape formalism	0.7	0.1	1.3	0.8	1.1	0.0
Bias correction	0.2	0.4	0.4	2.1		
Momentum scale	0.0		0.1		0.0	
Mass constraint	0.1	0.1	0.1	0.5	0.1	0.4
Background	0.1	0.3	0.2	0.8	0.7	4.0
Total	1.1	1.5	2.3	7.5	8.5	5.8

potential under-estimation of the statistical uncertainty. Therefore, the term $\sqrt{\sigma_{\text{pull}}^2 - 1} \cdot \sigma_{\text{stat}}$ is assigned as a systematic uncertainty. A relative uncertainty of 3×10^{-4} on the charged particle momentum scale [7] is propagated through the simulation. The resolution σ_{res} is varied within uncertainty and the resulting difference on the fitted parameters of the resolution function is then propagated to the masses and natural widths of the excited Ξ_c^0 states, which is found to be negligible. The magnitude of the energy-loss correction for charged particles is known to 10% accuracy [29]. In the study of Ref. [14], a correction of less than 0.01 MeV per track is estimated. A conservative estimation of 0.01 MeV per track is taken as the systematic uncertainty, which is also found to be negligible.

Mass constraints on the B^- and Λ_c^+ candidates are applied when calculating $M(\Lambda_c^+ K^-)$. The maximum change after varying the B^- or Λ_c^+ mass by one standard deviation is assigned as a systematic uncertainty. The systematic uncertainty due to the background is estimated by generating and fitting 300 pseudoexperiments, randomly varying the background yield according to a Poisson distribution while fixing the Ξ_c^0 yield, the parameters of the Ξ_c^0 model and the nonresonant yield. The average of the fitted values is calculated, and its difference from the nominal result is assigned as a systematic uncertainty.

A summary of the systematic uncertainties are listed in Table III. The uncertainties from different sources are uncorrelated and are added in quadrature to give the total systematic uncertainty. The significance of the $\Xi_c(2880)^0$ and $\Xi_c(2790)^0$ states is 3.8σ and 3.7σ , respectively, after taking the systematic uncertainties into account.

V. BRANCHING FRACTION

The relative branching fraction R_B of the $B^- \rightarrow \Lambda_c^+ \bar{\Lambda}_c^- K^-$ decay with respect to the $B^- \rightarrow D^+ D^- K^-$ channel is calculated as a ratio of efficiency-corrected yield divided by the corresponding charm decay branching fractions, expressed as

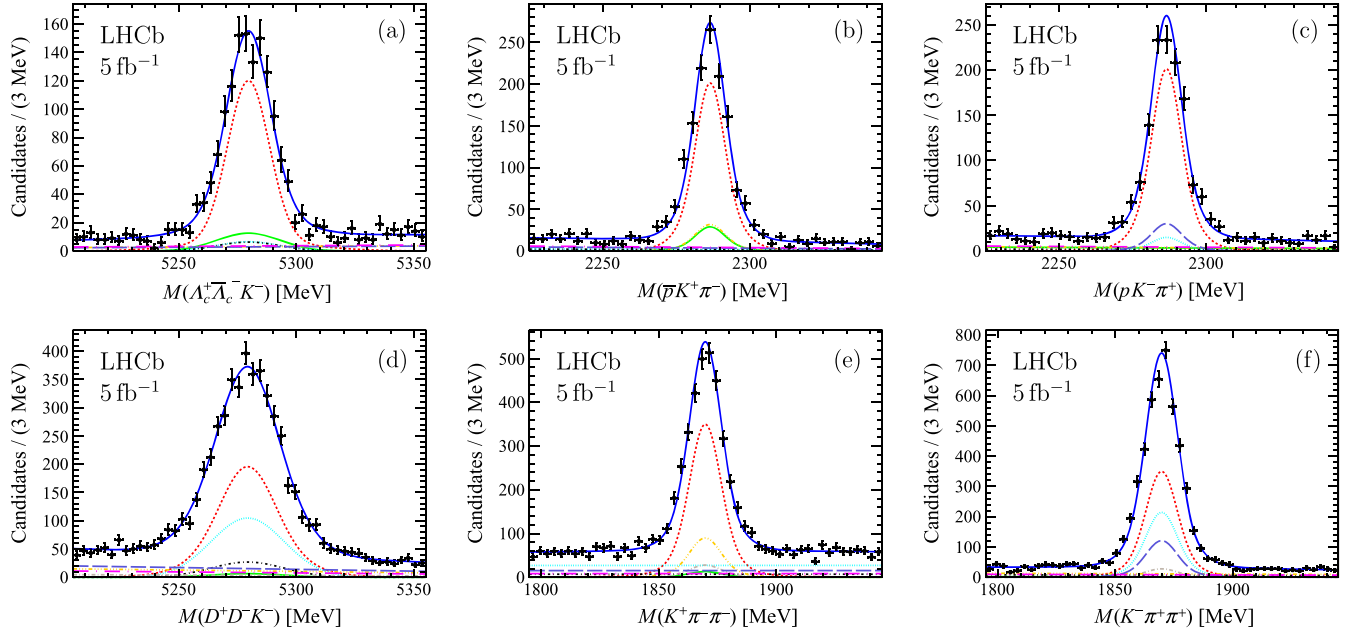


FIG. 5. Distributions of (a) $M(\Lambda_c^+ \bar{\Lambda}_c^- K^-)$, (b) $M(\bar{p} K^+ \pi^-)$ and (c) $M(p K^- \pi^+)$ in the $B^- \rightarrow \Lambda_c^+ \bar{\Lambda}_c^- K^-$ sample and distributions of (d) $M(D^+ D^- K^-)$, (e) $M(K^+ \pi^- \pi^-)$ and (f) $M(K^- \pi^+ \pi^+)$ in the $B^- \rightarrow D^+ D^- K^-$ sample. All selected events are triggered due to B^- candidates. The legend is the same as in Fig. 1, except replacing Λ_c^+ ($\bar{\Lambda}_c^-$) with D^+ (D^-) for the $B^- \rightarrow D^+ D^- K^-$ decay.

$$R_B = \frac{N(B^- \rightarrow \Lambda_c^+ \bar{\Lambda}_c^- K^-)}{N(B^- \rightarrow D^+ D^- K^-)} \times \frac{\epsilon_{\text{tot}}(B^- \rightarrow D^+ D^- K^-)}{\epsilon_{\text{tot}}(B^- \rightarrow \Lambda_c^+ \bar{\Lambda}_c^- K^-)} \times \frac{\mathcal{B}^2(D^+ \rightarrow K^- \pi^+ \pi^+)}{\mathcal{B}^2(\Lambda_c^+ \rightarrow p K^- \pi^+)}. \quad (5)$$

The yield of the signal and normalization channels is obtained from the 3D fit described in Sec. III. The charm decay branching fractions $\mathcal{B}(D^+ \rightarrow K^- \pi^+ \pi^+)$ [(9.38 ± 0.16)%] and $\mathcal{B}(\Lambda_c^+ \rightarrow p K^- \pi^+)$ [(6.28 ± 0.32)%] are obtained from Ref. [25].

In addition to the selection described in Sec. II, it is required that all selected signal events are triggered on the B^- candidate decay products for both signal and normalisation modes so that the trigger efficiencies can be estimated accurately. The projections of the 3D fit to the $B^- \rightarrow \Lambda_c^+ \bar{\Lambda}_c^- K^-$ spectra with these additional requirements are shown in Figs. 5(a)–5(c) and the measured yield is 977 ± 36 . For the normalisation decay $B^- \rightarrow D^+ D^- K^-$, a similar 3D fit is performed to the mass distributions of the B^- , D^+ and D^- candidates with the same fitting functions except replacing Λ_c with D wherever applicable. The fitted distributions are shown in Figs. 5(d)–5(f), and the yield of $B^- \rightarrow D^+ D^- K^-$ decay is 2212 ± 62 .

The total efficiency ϵ_{tot} is the product of the efficiencies due to the detector acceptance, trigger, reconstruction, offline preselection and multivariate selection. The efficiencies from different sources are estimated with a combination of simulation and data. Weights are assigned to the simulated events such that the track multiplicity

distribution agrees with the data. The tracking efficiency for charged tracks is estimated using data, and the difference between simulation and data is obtained from a correction table as a function of p_T , η and number of charged tracks [30]. The total efficiencies of the signal and normalisation decays are $(3.41 \pm 0.02) \times 10^{-4}$ and $(8.15 \pm 0.11) \times 10^{-4}$, respectively, where the uncertainties come from the statistics of the simulation samples. An alternative set of selections of the $B^- \rightarrow \Lambda_c^+ \bar{\Lambda}_c^- K^-$ signal with tighter criteria on p_T and looser criteria on B^- decay time is used as a cross-check, and the efficiency-corrected yield is found to be consistent with the baseline selections.

The systematic uncertainty on the relative branching fraction comes from uncertainties in signal yield determination and efficiency estimation. The working point of the BDT output is chosen to maximise the signal significance. The choice of BDT thresholds are varied and no significant bias is found. The average of the efficiency-corrected yield agrees with the nominal result within statistical uncertainties, and the maximum change in the central value is taken as a systematic uncertainty. Alternative assumptions are made when performing the 3D fits, including varying the fitting range, using fixed shapes from simulation for the signal in the fit, and varying the mass resolution for B decay backgrounds. The shifts in yield are taken as systematic uncertainties. The simulation sample is weighted to match the track multiplicity distribution of data, and the uncertainties of the weights are propagated to the efficiencies. The efficiency dependence on the decay phase space is studied in the $M(\bar{\Lambda}_c^- K^-)$ vs. $M(\Lambda_c^+ K^-)$ [$M(D^- K^-)$ vs.

TABLE IV. Relative systematic uncertainties of the branching fractions of signal, normalization channel, and their ratio R_B (in percent). Correlation between the two channels are considered.

Source	$B^- \rightarrow \Lambda_c^+ \bar{\Lambda}_c^- K^-$	$B^- \rightarrow D^+ D^- K^-$	R_B
BDT working point	1.5	0.4	1.6
Fit range	1.2	0.6	1.3
Detector resolution	0.0	0.3	0.3
Signal model	0.0	1.6	1.6
Simulation weighting	2.6	3.8	4.6
Decay phase space	0.1	0.2	0.3
PID resample	0.6	0.9	1.0
Detector parametrization	3.3	2.5	0.8
Trigger	5.6	4.9	7.5
Simulation sample size	0.9	1.2	1.5
Total			9.4

$M(D^+K^-)$ plane for the signal (normalization) decay. The efficiencies are calculated alternatively according to each candidate's decay phase space and the shift in central values is taken as a systematic uncertainty. The tracking efficiency has a negligible effect on the final results. The PID values in simulation are sampled to better agree with data using a dedicated tool [24]. An alternative template is used for the sampling and the shift in the efficiency-corrected yield is taken as a systematic uncertainty. The parametrization of the VELO materials, which influences IP-related variables, is tuned on simulation. The χ^2_{IP} distribution in simulation is scaled with parameters given by the $\Lambda_b^0 \rightarrow \Lambda_c^+ \pi^-$ sample, and the shift in R_B using the scaled simulation is assigned as a systematic uncertainty. The trigger efficiencies are estimated using the simulation as the baseline. They are also estimated using data, taking the events triggered independent of the B^- candidates. The estimated efficiencies between the two methods agree within statistical uncertainties, and the difference between efficiencies calculated using data and the nominal value is assigned as a systematic uncertainty. The uncertainty due to the limited simulation sample size is propagated to the final result. The systematic uncertainty on R_B is summarized in Table IV, and all the terms mentioned above are added in quadrature.

The ratio of branching fractions is measured to be

$$R_B = 2.36 \pm 0.11 \pm 0.22 \pm 0.25,$$

where the uncertainties are statistical, systematic and that due to uncertainties on the Λ_c^+ and D^+ branching fractions. This measurement is significantly improved with respect to $R_B = 2.23 \pm 0.78$ calculated using values from Ref. [25].

VI. SUMMARY

The $B^- \rightarrow \Lambda_c^+ \bar{\Lambda}_c^- K^-$ decay is studied for the first time in pp collisions using data collected by the LHCb

experiment, corresponding to an integrated luminosity of 5 fb^{-1} . In the $\Lambda_c^+ K^-$ invariant mass spectrum, two neutral excited charm baryon states, $\Xi_c(2923)^0$ and $\Xi_c(2939)^0$, are observed. Their masses and widths are in agreement with those of the states observed in a prompt $\Lambda_c^+ K^-$ measurement [7]. These new measurements confirm that the $\Xi_c(2930)^0$ state observed in $B^- \rightarrow \Lambda_c^+ \bar{\Lambda}_c^- K^-$ at B -factories is resolved into two separate states. No resonance structure is found at higher masses. Evidence for the $\Xi_c(2880)^0$ state is found with a significance of 3.8σ . In addition, evidence of a new $\Xi_c(2790)^0 \rightarrow \Lambda_c^+ K^-$ decay is found with a significance of 3.7σ .

The relative branching fraction of $B^- \rightarrow \Lambda_c^+ \bar{\Lambda}_c^- K^-$ is measured with respect to $B^- \rightarrow D^+ D^- K^-$ as $R_B = 2.36 \pm 0.11 \pm 0.22 \pm 0.25$, where the uncertainties are statistical, systematic and that due to the charm decay branching fraction. This is the most precise measurement to date of this ratio.

ACKNOWLEDGMENTS

We express our gratitude to our colleagues in the CERN accelerator departments for the excellent performance of the LHC. We thank the technical and administrative staff at the LHCb institutes. We acknowledge support from CERN and from the national agencies: CAPES, CNPq, FAPERJ and FINEP (Brazil); MOST and NSFC (China); CNRS/IN2P3 (France); BMBF, DFG and MPG (Germany); INFN (Italy); NWO (Netherlands); MNiSW and NCN (Poland); MEN/IFA (Romania); MICINN (Spain); SNSF and SER (Switzerland); NASU (Ukraine); STFC (United Kingdom); DOE NP and NSF (USA). We acknowledge the computing resources that are provided by CERN, IN2P3 (France), KIT and DESY (Germany), INFN (Italy), SURF (Netherlands), PIC (Spain), GridPP (United Kingdom), CSCS (Switzerland), IFIN-HH (Romania), CBPF (Brazil), Polish WLCG (Poland) and NERSC (USA). We are indebted to the communities behind the multiple open-source software packages on which we depend. Individual groups or members have received support from ARC and ARDC (Australia); Minciencias (Colombia); AvH Foundation (Germany); EPLANET, Marie Skłodowska-Curie Actions and ERC (European Union); A*MIDEX, ANR, IPhU and Labex P2IO, and Région Auvergne-Rhône-Alpes (France); Key Research Program of Frontier Sciences of CAS, CAS PIFI, CAS CCEPP, Fundamental Research Funds for the Central Universities, and Sci. & Tech. Program of Guangzhou (China); GVA, XuntaGal, GENCAT and Prog. Atracción Talento, CM (Spain); SRC (Sweden); the Leverhulme Trust, the Royal Society and UKRI (United Kingdom).

- [1] B. Aubert *et al.* (BABAR Collaboration), A study of $\bar{B} \rightarrow \Xi_c \bar{\Lambda}_c^-$ and $\bar{B} \rightarrow \Lambda_c^+ \bar{\Lambda}_c^- \bar{K}$ decays at BABAR, *Phys. Rev. D* **77**, 031101 (2008).
- [2] Y. B. Li *et al.* (Belle Collaboration), Observation of $\Xi_c(2930)^0$ and updated measurement of $B^- \rightarrow K^- \Lambda_c^+ \bar{\Lambda}_c^-$ at Belle, *Eur. Phys. J. C* **78**, 252 (2018).
- [3] Y. B. Li *et al.* (Belle Collaboration), Evidence of a structure in $\bar{K}^0 \Lambda_c^+$ consistent with a charged $\Xi_c(2930)^+$, and updated measurement of $\bar{B}^0 \rightarrow \bar{K}^0 \Lambda_c^+ \bar{\Lambda}_c^-$ at Belle, *Eur. Phys. J. C* **78**, 928 (2018).
- [4] R. Aaij *et al.* (LHCb Collaboration), Observation of Five New Narrow Ω_c^0 States Decaying to $\Xi_c^+ K^-$, *Phys. Rev. Lett.* **118**, 182001 (2017).
- [5] R. Aaij *et al.* (LHCb Collaboration), Observation of the Doubly Charmed Baryon Ξ_{cc}^{++} , *Phys. Rev. Lett.* **119**, 112001 (2017).
- [6] R. Aaij *et al.* (LHCb Collaboration), First Observation of the Doubly Charmed Baryon Decay $\Xi_{cc}^{++} \rightarrow \Xi_c^+ \pi^+$, *Phys. Rev. Lett.* **121**, 162002 (2018).
- [7] R. Aaij *et al.* (LHCb Collaboration), Observation of New Ξ_c^0 Baryons Decaying to $\Lambda_c^+ K^-$, *Phys. Rev. Lett.* **124**, 222001 (2020).
- [8] K.-L. Wang, L.-Y. Xiao, and X.-H. Zhong, Understanding the newly observed Ξ_c^0 states through their decays, *Phys. Rev. D* **102**, 034029 (2020).
- [9] G. Pakhlova *et al.* (Belle Collaboration), Observation of a Near-Threshold Enhancement in the $e^+ e^- \rightarrow \Lambda_c^+ \bar{\Lambda}_c^-$ Cross Section using Initial-State Radiation, *Phys. Rev. Lett.* **101**, 172001 (2008).
- [10] M. Ablikim *et al.* (BESIII Collaboration), Precision Measurement of the $e^+ e^- \rightarrow \Lambda_c^+ \bar{\Lambda}_c^-$ Cross Section near Threshold, *Phys. Rev. Lett.* **120**, 132001 (2018).
- [11] A. A. Alves Jr. *et al.* (LHCb Collaboration), The LHCb detector at the LHC, *J. Instrum.* **3**, S08005 (2008).
- [12] LHCb Collaboration, LHCb detector performance, *Int. J. Mod. Phys. A* **30**, 1530022 (2015).
- [13] R. Aaij *et al.* (LHCb Collaboration), Measurements of the Λ_b^0 , Ξ_b^- , and Ω_b^- Baryon Masses, *Phys. Rev. Lett.* **110**, 182001 (2013).
- [14] R. Aaij *et al.* (LHCb Collaboration), Precision measurement of D meson mass differences, *J. High Energy Phys.* **06** (2013) 065.
- [15] T. Sjöstrand, S. Mrenna, and P. Skands, A brief introduction to PYTHIA 8.1, *Comput. Phys. Commun.* **178**, 852 (2008).
- [16] I. Belyaev *et al.*, Handling of the generation of primary events in Gauss, the LHCb simulation framework, *J. Phys. Conf. Ser.* **331**, 032047 (2011).
- [17] D. J. Lange, The EvtGen particle decay simulation package, *Nucl. Instrum. Methods Phys. Res., Sect. A* **462**, 152 (2001).
- [18] N. Davidson, T. Przedzinski, and Z. Was, PHOTOS interface in c++: Technical and physics documentation, *Comput. Phys. Commun.* **199**, 86 (2016).
- [19] J. Allison *et al.* (Geant4 Collaboration), Geant4 developments and applications, *IEEE Trans. Nucl. Sci.* **53**, 270 (2006); S. Agostinelli *et al.* (Geant4 Collaboration), Geant4: A simulation toolkit, *Nucl. Instrum. Methods Phys. Res., Sect. A* **506**, 250 (2003).
- [20] M. Clemencic, G. Corti, S. Easo, C. R. Jones, S. Miglioranza, M. Pappagallo, and P. Robbe, The LHCb simulation application, Gauss: Design, evolution and experience, *J. Phys. Conf. Ser.* **331**, 032023 (2011).
- [21] L. Breiman, J. H. Friedman, R. A. Olshen, and C. J. Stone, *Classification and Regression Trees* (Wadsworth International Group, Belmont, California, USA, 1984).
- [22] Y. Freund and R. E. Schapire, A decision-theoretic generalization of on-line learning and an application to boosting, *J. Comput. Syst. Sci.* **55**, 119 (1997).
- [23] H. Voss, A. Hoecker, J. Stelzer, and F. Tegenfeldt, TMVA—Toolkit for multivariate data analysis with ROOT, *Proc. Sci. ACAT2007* (2007) 040; A. Hoecker *et al.*, TMVA 4—Toolkit for multivariate data analysis with ROOT. Users guide, [arXiv:physics/0703039](https://arxiv.org/abs/physics/0703039).
- [24] R. Aaij *et al.*, Selection and processing of calibration samples to measure the particle identification performance of the LHCb experiment in Run 2, *EPJ Tech. Instrum.* **6**, 1 (2019).
- [25] P. A. Zyla *et al.* (Particle Data Group), Review of particle physics, *Prog. Theor. Exp. Phys.* **2020**, 083C01 (2020).
- [26] M. Pivk and F. R. Le Diberder, sPlot: A statistical tool to unfold data distributions, *Nucl. Instrum. Methods Phys. Res., Sect. A* **555**, 356 (2005).
- [27] R. Aaij *et al.* (LHCb Collaboration), Amplitude analysis of $B^+ \rightarrow J/\psi \phi K^+$ decays, *Phys. Rev. D* **95**, 012002 (2017).
- [28] I. J. R. Aitchison, K-matrix formalism for overlapping resonances, *Nucl. Phys.* **A189**, 417 (1972).
- [29] R. Aaij *et al.* (LHCb Collaboration), Prompt K_S^0 production in $p p$ collisions at $\sqrt{s} = 0.9$ TeV, *Phys. Lett. B* **693**, 69 (2010).
- [30] LHCb Collaboration, Measurement of the track reconstruction efficiency at LHCb, *J. Instrum.* **10**, P02007 (2015).

R. Aaij^{1b,32}, A. S. W. Abdelmotteleb^{1b,50}, C. Abellan Beteta⁴⁴, F. Abudinén^{1b,50}, T. Ackernley^{1b,54}, B. Adeva^{1b,40}, M. Adinolfi^{1b,48}, P. Adlarson^{1b,77}, H. Afsharnia⁹, C. Agapopoulou^{1b,13}, C. A. Aidala^{1b,78}, S. Aiola^{1b,25}, Z. Ajaltouni⁹, S. Akar^{1b,59}, K. Akiba^{1b,32}, J. Albrecht^{1b,15}, F. Alessio^{1b,42}, M. Alexander^{1b,53}, A. Alfonso Alberio^{1b,39}, Z. Aliouche^{1b,56}, P. Alvarez Cartelle^{1b,49}, R. Amalric^{1b,13}, S. Amato^{1b,2}, J. L. Amey^{1b,48}, Y. Amhis^{1b,11,42}, L. An^{1b,42}, L. Anderlini^{1b,22}, M. Andersson^{1b,44}, A. Andreianov^{1b,38}, M. Andreotti^{1b,21}, D. Andreou^{1b,62}, D. Ao^{1b,6}, F. Archilli^{1b,17}, A. Artamonov^{1b,38}, M. Artuso^{1b,62}, E. Aslanides^{1b,10}, M. Atzeni^{1b,44}, B. Audurier^{1b,12}, S. Bachmann^{1b,17}, M. Bachmayer^{1b,43}, J. J. Back^{1b,50}, A. Bailly-reyre^{1b,13}, P. Baladrón Rodríguez^{1b,40}, V. Balagura^{1b,12}, W. Baldini^{1b,21}, J. Baptista de Souza Leite^{1b,1}, M. Barbetti^{1b,22,b}, R. J. Barlow^{1b,56}, S. Barsuk^{1b,11}, W. Barter^{1b,55}, M. Bartolini^{1b,49}, F. Baryshnikov^{1b,38}, J. M. Basels^{1b,14}

G. Bassi^{29,c} B. Batsukh⁴ A. Battig¹⁵ A. Bay⁴³ A. Beck⁵⁰ M. Becker¹⁵ F. Bedeschi²⁹ I. B. Bediaga¹
A. Beiter⁶² V. Belavin³⁸ S. Belin⁴⁰ V. Bellee⁴⁴ K. Belous³⁸ I. Belov³⁸ I. Belyaev³⁸ G. Benane¹⁰
G. Bencivenni²³ E. Ben-Haim¹³ A. Berezhnoy³⁸ R. Bernet⁴⁴ S. Bernet Andres⁷⁶ D. Berninghoff¹⁷
H. C. Bernstein⁶² C. Bertella⁵⁶ A. Bertolin²⁸ C. Betancourt⁴⁴ F. Betti⁴² Ia. Bezshyiko⁴⁴ S. Bhasin⁴⁸
J. Bhom³⁵ L. Bian⁶⁸ M. S. Bieker¹⁵ N. V. Biesuz²¹ S. Bifani⁴⁷ P. Billoir¹³ A. Biolchini³² M. Birch⁵⁵
F. C. R. Bishop⁴⁹ A. Bitadze⁵⁶ A. Bizzeti¹⁵ M. P. Blago⁴⁹ T. Blake⁵⁰ F. Blanc⁴³ J. E. Blank¹⁵ S. Blusk⁶²
D. Bobulska⁵³ J. A. Boelhauve¹⁵ O. Boente Garcia¹² T. Boettcher⁵⁹ A. Boldyrev³⁸ C. S. Bolognani⁷⁴
R. Bolzonella^{21,d} N. Bondar^{38,42} F. Borgato²⁸ S. Borghi⁵⁶ M. Borsato¹⁷ J. T. Borsuk³⁵ S. A. Bouchiba⁴³
T. J. V. Bowcock⁵⁴ A. Boyer⁴² C. Bozzi²¹ M. J. Bradley⁵⁵ S. Braun⁶⁰ A. Brea Rodriguez⁴⁰ J. Brodzicka³⁵
A. Brossa Gonzalo⁴⁰ J. Brown⁵⁴ D. Brundu²⁷ A. Buonaura⁴⁴ L. Buonincontri²⁸ A. T. Burke⁵⁶ C. Burr⁴²
A. Bursche⁶⁶ A. Butkevich³⁸ J. S. Butter³² J. Buytaert⁴² W. Byczynski⁴² S. Cadeddu²⁷ H. Cai⁶⁸
R. Calabrese^{21,d} L. Calefice¹⁵ S. Cali²³ R. Calladine⁴⁷ M. Calvi^{26,e} M. Calvo Gomez⁷⁶ P. Campana²³
D. H. Campora Perez⁷⁴ A. F. Campoverde Quezada⁶ S. Capelli^{26,e} L. Capriotti²⁰ A. Carbone^{20,f} G. Carboni³¹
R. Cardinale^{24,g} A. Cardini²⁷ P. Carniti^{26,e} L. Carus¹⁴ A. Casais Vidal⁴⁰ R. Caspary¹⁷ G. Casse⁵⁴
M. Cattaneo⁴² G. Cavallero⁴² V. Cavallini^{21,d} S. Celani⁴³ J. Cerasoli¹⁰ D. Cervenkov⁵⁷ A. J. Chadwick⁵⁴
M. G. Chapman⁴⁸ M. Charles¹³ Ph. Charpentier⁴² C. A. Chavez Barajas⁵⁴ M. Chefdeville⁸ C. Chen³
S. Chen⁴ A. Chernov³⁵ S. Chernyshenko⁴⁶ V. Chobanova⁴⁰ S. Cholak⁴³ M. Chruszcz³⁵ A. Chubykin³⁸
V. Chulikov³⁸ P. Ciambrone²³ M. F. Cicala⁵⁰ X. Cid Vidal⁴⁰ G. Ciezarek⁴² G. Ciullo^{21,d} P. E. L. Clarke⁵²
M. Clemencic⁴² H. V. Cliff⁴⁹ J. Closier⁴² J. L. Cobbedick⁵⁶ V. Coco⁴² J. A. B. Coelho¹¹ J. Cogan¹⁰
E. Cogneras⁹ L. Cojocariu³⁷ P. Collins⁴² T. Colombo⁴² L. Congedo¹⁹ A. Contu²⁷ N. Cooke⁴⁷
I. Corredoira⁴⁰ G. Corti⁴² B. Couturier⁴² D. C. Craik⁴⁴ M. Cruz Torres^{1,h} R. Currie⁵² C. L. Da Silva⁶¹
S. Dadabaev³⁸ L. Dai⁶⁵ X. Dai⁵ E. Dall'Occo¹⁵ J. Dalseno⁴⁰ C. D'Ambrosio⁴² J. Daniel⁹ A. Danilina³⁸
P. d'Argent¹⁵ J. E. Davies⁵⁶ A. Davis⁵⁶ O. De Aguiar Francisco⁵⁶ J. de Boer⁴² K. De Bruyn⁷³ S. De Capua⁵⁶
M. De Cian⁴³ U. De Freitas Carneiro Da Graca¹ E. De Lucia²³ J. M. De Miranda¹ L. De Paula² M. De Serio^{19,i}
D. De Simone⁴⁴ P. De Simone²³ F. De Vellis¹⁵ J. A. de Vries⁷⁴ C. T. Dean⁶¹ F. Debernardis^{19,i} D. Decamp⁸
V. Dedu¹⁰ L. Del Buono¹³ B. Delaney⁵⁸ H.-P. Dembinski¹⁵ V. Denysenko⁴⁴ O. Deschamps⁹ F. Dettori^{27,j}
B. Dey⁷¹ P. Di Nezza²³ I. Diachkov³⁸ S. Didenko³⁸ L. Dieste Maronas⁴⁰ S. Ding⁶² V. Dobishuk⁴⁶
A. Dolmatov³⁸ C. Dong³ A. M. Donohoe¹⁸ F. Dordei²⁷ A. C. dos Reis¹ L. Douglas⁵³ A. G. Downes⁸
P. Duda⁷⁵ M. W. Dudek³⁵ L. Dufour⁴² V. Duk⁷² P. Durante⁴² M. M. Duras⁷⁵ J. M. Durham⁶¹ D. Dutta⁵⁶
A. Dziurda³⁵ A. Dzyuba³⁸ S. Easo⁵¹ U. Egede⁶³ V. Egorychev³⁸ S. Eidelman^{38,a} C. Eirea Orro⁴⁰
S. Eisenhardt⁵² E. Ejopu⁵⁶ S. Ek-In⁴³ L. Eklund⁷⁷ S. Ely⁶² A. Ene³⁷ E. Epple⁵⁹ S. Escher¹⁴ J. Eschle⁴⁴
S. Esen⁴⁴ T. Evans⁵⁶ F. Fabiano^{27,j} L. N. Falcao¹ Y. Fan⁶ B. Fang⁶⁸ L. Fantini^{72,k} M. Faria⁴³ S. Farry⁵⁴
D. Fazzini^{26,e} L. F. Felkowski⁷⁵ M. Feo⁴² M. Fernandez Gomez⁴⁰ A. D. Fernandez⁶⁰ F. Ferrari²⁰
L. Ferreira Lopes⁴³ F. Ferreira Rodrigues² S. Ferreres Sole³² M. Ferrillo⁴⁴ M. Ferro-Luzzi⁴² S. Filippov³⁸
R. A. Fini¹⁹ M. Fiorini^{21,d} M. Firlej³⁴ K. M. Fischer⁵⁷ D. S. Fitzgerald⁷⁸ C. Fitzpatrick⁵⁶ T. Fiutowski³⁴
F. Fleuret¹² M. Fontana¹³ F. Fontanelli^{24,g} R. Forty⁴² D. Foulds-Holt⁴⁹ V. Franco Lima⁵⁴
M. Franco Sevilla⁶⁰ M. Frank⁴² E. Franzoso^{21,d} G. Frau¹⁷ C. Frei⁴² D. A. Friday⁵³ J. Fu⁶ Q. Fuehring¹⁵
T. Fulghesu¹³ E. Gabriel³² G. Galati^{19,i} M. D. Galati³² A. Gallas Torreira⁴⁰ D. Galli^{20,f} S. Gambetta^{52,42}
Y. Gan³ M. Gandelman² P. Gandini²⁵ Y. Gao⁷ Y. Gao⁵ M. Garau^{27,j} L. M. Garcia Martin⁵⁰
P. Garcia Moreno³⁹ J. Garcia Pardiñas^{26,e} B. Garcia Plana⁴⁰ F. A. Garcia Rosales¹² L. Garrido³⁹ C. Gaspar⁴²
R. E. Geertsema³² D. Gerick¹⁷ L. L. Gerken¹⁵ E. Gersabeck⁵⁶ M. Gersabeck⁵⁶ T. Gershon⁵⁰
L. Giambastiani²⁸ V. Gibson⁴⁹ H. K. Gienza³⁶ A. L. Gilman⁵⁷ M. Giovannetti^{23,l} A. Gioventù⁴⁰
P. Gironella Gironell³⁹ C. Giugliano^{21,d} M. A. Giza³⁵ K. Gizdov⁵² E. L. Gkougkousis⁴² V. V. Gligorov^{13,42}
C. Göbel⁶⁴ E. Golobardes⁷⁶ D. Golubkov³⁸ A. Golutvin^{55,38} A. Gomes^{1,m} S. Gomez Fernandez³⁹
F. Goncalves Abrantes⁵⁷ M. Goncerz³⁵ G. Gong³ I. V. Gorelov³⁸ C. Gotti²⁶ J. P. Grabowski⁷⁰
T. Grammatico¹³ L. A. Granado Cardoso⁴² E. Graugés³⁹ E. Graverini⁴³ G. Graziani⁴³ A. T. Grecu³⁷
L. M. Greeven³² N. A. Grieser⁴ L. Grillo⁵³ S. Gromov³⁸ B. R. Gruberg Cazon⁵⁷ C. Gu³ M. Guarise^{21,d}
M. Guittiere¹¹ P. A. Günther¹⁷ E. Gushchin³⁸ A. Guth¹⁴ Y. Guz³⁸ T. Gys⁴² T. Hadavizadeh⁶³ G. Haefeli⁴³
C. Haen⁴² J. Haimberger⁴² S. C. Haines⁴⁹ T. Halewood-leagas⁵⁴ M. M. Halvorsen⁴² P. M. Hamilton⁶⁰

J. Hammerich⁵⁴ Q. Han⁷ X. Han¹⁷ E. B. Hansen⁵⁶ S. Hansmann-Menzemer¹⁷ L. Hao⁶ N. Harnew⁵⁷
T. Harrison⁵⁴ C. Hasse⁴² M. Hatch⁴² J. He^{6,n} K. Heijhoff³² C. Henderson⁵⁹ R. D. L. Henderson^{63,50}
A. M. Hennequin⁵⁸ K. Hennessy⁵⁴ L. Henry⁴² J. Herd⁵⁵ J. Heuel¹⁴ A. Hicheur² D. Hill⁴³ M. Hilton⁵⁶
S. E. Hollitt¹⁵ J. Horswill⁵⁶ R. Hou⁷ Y. Hou⁸ J. Hu¹⁷ J. Hu⁶⁶ W. Hu⁵ X. Hu³ W. Huang⁶ X. Huang⁶⁸
W. Hulsbergen³² R. J. Hunter⁵⁰ M. Hushchyn³⁸ D. Hutchcroft⁵⁴ P. Ibis¹⁵ M. Idzik³⁴ D. Ilin³⁸ P. Iiten⁵⁹
A. Inglessi³⁸ A. Iniukhin³⁸ A. Ishteev³⁸ K. Ivshin³⁸ R. Jacobsson⁴² H. Jage¹⁴ S. J. Jaimes Elles⁴¹
S. Jakobsen⁴² E. Jans³² B. K. Jashal⁴¹ A. Jawahery⁶⁰ V. Jevtic¹⁵ E. Jiang⁶⁰ X. Jiang^{4,6} Y. Jiang⁶
M. John⁵⁷ D. Johnson⁵⁸ C. R. Jones⁴⁹ T. P. Jones⁵⁰ B. Jost⁴² N. Jurik⁴² I. Juszcak³⁵ S. Kandybei⁴⁵
Y. Kang³ M. Karacson⁴² D. Karpenkov³⁸ M. Karpov³⁸ J. W. Kautz⁵⁹ F. Keizer⁴² D. M. Keller⁶²
M. Kenzie⁵⁰ T. Ketel³² B. Khanji¹⁵ A. Kharisova³⁸ S. Kholodenko³⁸ G. Khreich¹¹ T. Kim¹⁴
V. S. Kirsebom⁴³ O. Kitouni⁵⁸ S. Klaver³³ N. Kleijne^{29,c} K. Klimaszewski³⁶ M. R. Kmiec³⁶ S. Koliiiev⁴⁶
A. Kondybayeva³⁸ A. Konoplyannikov³⁸ P. Kopciewicz³⁴ R. Kopečna¹⁷ P. Koppenburg³² M. Korolev³⁸
I. Kostiuk^{32,46} O. Kot⁴⁶ S. Kotriakhova³⁸ A. Kozachuk³⁸ P. Kravchenko³⁸ L. Kravchuk³⁸ R. D. Krawczyk⁴²
M. Krepš⁵⁰ S. Kretschmar¹⁴ P. Krokovny³⁸ W. Krupa³⁴ W. Krzemien³⁶ J. Kubat¹⁷ S. Kubis⁷⁵
W. Kucewicz^{35,34} M. Kucharczyk³⁵ V. Kudryavtsev³⁸ A. Kupsc⁷⁷ D. Lacarrere⁴² G. Lafferty⁵⁶ A. Lai²⁷
A. Lampis^{27,j} D. Lancierini⁴⁴ C. Landesa Gomez⁴⁰ J. J. Lane⁵⁶ R. Lane⁴⁸ G. Lanfranchi²³
C. Langenbruch¹⁴ J. Langer¹⁵ O. Lantwin³⁸ T. Latham⁵⁰ F. Lazzari^{29,o} M. Lazzaroni^{25,p} R. Le Gac¹⁰
S. H. Lee⁷⁸ R. Lefèvre⁹ A. Leflat³⁸ S. Legotin³⁸ P. Lenisa^{21,d} O. Leroy¹⁰ T. Lesiak³⁵ B. Leverington¹⁷
A. Li³ H. Li⁶⁶ K. Li⁷ P. Li¹⁷ P.-R. Li⁶⁷ S. Li⁷ T. Li⁴ T. Li⁶⁶ Y. Li⁴ Z. Li⁶² X. Liang⁶² C. Lin⁶
T. Lin⁵¹ R. Lindner⁴² V. Lisovskyi¹⁵ R. Litvinov^{27,j} G. Liu⁶⁶ H. Liu⁶ Q. Liu⁶ S. Liu^{4,6} A. Lobo Salvia³⁹
A. Loi²⁷ R. Lollini⁷² J. Lomba Castro⁴⁰ I. Longstaff⁵³ J. H. Lopes² A. Lopez Huertas³⁹ S. López Soliño⁴⁰
G. H. Lovell⁴⁹ Y. Lu^{4,q} C. Lucarelli^{22,b} D. Lucchesi^{28,r} S. Luchuk³⁸ M. Lucio Martinez⁷⁴
V. Lukashenko^{32,46} Y. Luo³ A. Lupato⁵⁶ E. Luppi^{21,d} A. Lusiani^{29,c} K. Lynch¹⁸ X.-R. Lyu⁶ L. Ma⁴
R. Ma⁶ S. Maccolini²⁰ F. Machefert¹¹ F. Maciuc³⁷ I. Mackay⁵⁷ V. Macko⁴³ P. Mackowiak¹⁵
L. R. Madhan Mohan⁴⁸ A. Maevskiy³⁸ D. Maisuzenko³⁸ M. W. Majewski³⁴ J. J. Malczewski³⁵ S. Malde⁵⁷
B. Malecki^{35,42} A. Malinin³⁸ T. Maltsev³⁸ G. Manca^{27,j} G. Mancinelli¹⁰ C. Mancuso^{11,25,p} D. Manuzzi²⁰
C. A. Manzari⁴⁴ D. Marangotto^{25,p} J. F. Marchand⁸ U. Marconi²⁰ S. Mariani^{22,b} C. Marin Benito³⁹
J. Marks¹⁷ A. M. Marshall⁴⁸ P. J. Marshall⁵⁴ G. Martelli^{72,k} G. Martellotti³⁰ L. Martinazzoli^{42,e}
M. Martinelli^{26,e} D. Martinez Santos⁴⁰ F. Martinez Vidal⁴¹ A. Massafferri¹ M. Materok¹⁴ R. Matev⁴²
A. Mathad⁴⁴ V. Matiunin³⁸ C. Matteuzzi²⁶ K. R. Mattioli¹² A. Mauri³² E. Maurice¹² J. Mauricio³⁹
M. Mazurek⁴² M. McCann⁵⁵ L. Mcconnell¹⁸ T. H. McGrath⁵⁶ N. T. McHugh⁵³ A. McNab⁵⁶ R. McNulty¹⁸
J. V. Mead⁵⁴ B. Meadows⁵⁹ G. Meier¹⁵ D. Melnychuk³⁶ S. Meloni^{26,e} M. Merk^{32,74} A. Merli^{25,p}
L. Meyer Garcia² D. Miao^{4,6} M. Mikhasenko^{70,s} D. A. Milanes⁶⁹ E. Millard⁵⁰ M. Milovanovic⁴²
M.-N. Minard^{8,a} A. Minotti^{26,e} T. Miralles⁹ S. E. Mitchell⁵² B. Mitreska⁵⁶ D. S. Mitzel¹⁵ A. Mödden¹⁵
R. A. Mohammed⁵⁷ R. D. Moise¹⁴ S. Mokhnenko³⁸ T. Mombächer⁴⁰ M. Monk^{50,63} I. A. Monroy⁶⁹
S. Monteil⁹ M. Morandin²⁸ G. Morello²³ M. J. Morello^{29,c} J. Moron³⁴ A. B. Morris⁷⁰ A. G. Morris⁵⁰
R. Mountain⁶² H. Mu³ E. Muhammad⁵⁰ F. Muheim⁵² M. Mulder⁷³ K. Müller⁴⁴ C. H. Murphy⁵⁷
D. Murray⁵⁶ R. Murta⁵⁵ P. Muzzetto^{27,j} P. Naik⁴⁸ T. Nakada⁴³ R. Nandakumar⁵¹ T. Nanut⁴² I. Nasteva²
M. Needham⁵² N. Neri^{25,p} S. Neubert⁷⁰ N. Neufeld⁴² P. Neustroev³⁸ R. Newcombe⁵⁵ J. Nicolini^{15,11}
E. M. Niel⁴³ S. Nieswand¹⁴ N. Nikitin³⁸ N. S. Nolte⁵⁸ C. Normand^{8,27,j} J. Novoa Fernandez⁴⁰ C. Nunez⁷⁸
A. Oblakowska-Mucha³⁴ V. Obraztsov³⁸ T. Oeser¹⁴ D. P. O'Hanlon⁴⁸ S. Okamura^{21,d} R. Oldeman^{27,j}
F. Oliva⁵² C. J. G. Onderwater⁷³ R. H. O'Neil⁵² J. M. Otalora Goicochea² T. Ovsianikova³⁸ P. Owen⁴⁴
A. Oyanguren⁴¹ O. Ozcelik⁵² K. O. Padeken⁷⁰ B. Pagare⁵⁰ P. R. Pais⁴² T. Pajero⁵⁷ A. Palano¹⁹
M. Palutan²³ Y. Pan⁵⁶ G. Panshin³⁸ L. Paolucci⁵⁰ A. Papanestis⁵¹ M. Pappagallo^{19,i} L. L. Pappalardo^{21,d}
C. Pappenheimer⁵⁹ W. Parker⁶⁰ C. Parkes⁵⁶ B. Passalacqua^{21,d} G. Passaleva²² A. Pastore¹⁹ M. Patel⁵⁵
C. Patrignani^{20,f} C. J. Pawley⁷⁴ A. Pearce⁴² A. Pellegrino³² M. Pepe Altarelli⁴² S. Perazzini²⁰ D. Pereima³⁸
A. Pereiro Castro⁴⁰ P. Perret⁹ M. Petric⁵³ K. Petridis⁴⁸ A. Petrolini^{24,g} A. Petrov³⁸ S. Petrucci⁵² M. Petruzzo²⁵
H. Pham⁶² A. Philippov³⁸ R. Piandani⁶ L. Pica^{29,c} M. Piccini⁷² B. Pietrzyk⁸ G. Pietrzyk¹¹ M. Pili⁵⁷
D. Pinci³⁰ F. Pisani⁴² M. Pizzichemi^{26,42,e} V. Placinta³⁷ J. Plews⁴⁷ M. Plo Casasus⁴⁰ F. Polci^{13,42}

M. Poli Lener²³, M. Poliakova,⁶² A. Poluektov¹⁰, N. Polukhina³⁸, I. Polyakov⁴², E. Polycarpo², S. Ponce⁴²,
D. Popov^{6,42}, S. Popov³⁸, S. Poslavskii³⁸, K. Prasanth³⁵, L. Promberger¹⁷, C. Prouve⁴⁰, V. Pugatch⁴⁶,
V. Puill¹¹, G. Punzi^{29,t}, H. R. Qi³, W. Qian⁶, N. Qin³, S. Qu³, R. Quagliani⁴³, N. V. Raab¹⁸,
R. I. Rabadan Trejo⁶, B. Rachwal³⁴, J. H. Rademacker⁴⁸, R. Rajagopalan,⁶² M. Rama²⁹, M. Ramos Pernas⁵⁰,
M. S. Rangel², F. Ratnikov³⁸, G. Raven^{33,42}, M. Rebollo De Miguel⁴¹, F. Redi⁴², J. Reich⁴⁸, F. Reiss⁵⁶,
C. Remon Alepuz,⁴¹ Z. Ren³, P. K. Resmi¹⁰, R. Ribatti^{29,c}, A. M. Ricci²⁷, S. Ricciardi⁵¹, K. Richardson⁵⁸,
M. Richardson-Slipper⁵², K. Rinnert⁵⁴, P. Robbe¹¹, G. Robertson⁵², A. B. Rodrigues⁴³, E. Rodrigues⁵⁴,
E. Rodriguez Fernandez⁴⁰, J. A. Rodriguez Lopez⁶⁹, E. Rodriguez Rodriguez⁴⁰, D. L. Rolf⁴², A. Rollings⁵⁷,
P. Roloff⁴², V. Romanovskiy³⁸, M. Romero Lamas⁴⁰, A. Romero Vidal⁴⁰, J. D. Roth,^{78,a} M. Rotondo²³,
M. S. Rudolph⁶², T. Ruf⁴², R. A. Ruiz Fernandez⁴⁰, J. Ruiz Vidal,⁴¹ A. Ryzhikov³⁸, J. Ryzka³⁴,
J. J. Saborido Silva⁴⁰, N. Sagidova³⁸, N. Sahoo⁴⁷, B. Saitta^{27,j}, M. Salomoni⁴², C. Sanchez Gras³²,
I. Sanderswood⁴¹, R. Santacesaria³⁰, C. Santamarina Rios⁴⁰, M. Santimaria²³, E. Santovetti^{31,l}, D. Saranin³⁸,
G. Sarpis¹⁴, M. Sarpis⁷⁰, A. Sarti³⁰, C. Satriano^{30,u}, A. Satta³¹, M. Saur¹⁵, D. Savrina³⁸, H. Sazak⁹,
L. G. Scantlebury Smead⁵⁷, A. Scarabotto¹³, S. Schael¹⁴, S. Scherl⁵⁴, M. Schiller⁵³, H. Schindler⁴²,
M. Schmelling¹⁶, B. Schmidt⁴², S. Schmitt¹⁴, O. Schneider⁴³, A. Schopper⁴², M. Schubiger³², S. Schulte⁴³,
M. H. Schune¹¹, R. Schwemmer⁴², B. Sciascia^{23,42}, A. Sciuccati⁴², S. Sellam⁴⁰, A. Semennikov³⁸,
M. Senghi Soares³³, A. Sergi^{24,g}, N. Serra⁴⁴, L. Sestini²⁸, A. Seuthe¹⁵, Y. Shang⁵, D. M. Shangase⁷⁸,
M. Shapkin³⁸, I. Shchemerov³⁸, L. Shchutska⁴³, T. Shears⁵⁴, L. Shekhtman³⁸, Z. Shen⁵, S. Sheng^{4,6},
V. Shevchenko³⁸, B. Shi⁶, E. B. Shields^{26,e}, Y. Shimizu¹¹, E. Shmanin³⁸, R. Shorkin³⁸, J. D. Shupperd⁶²,
B. G. Siddi^{21,d}, R. Silva Coutinho⁶², G. Simi²⁸, S. Simone^{19,i}, M. Singla⁶³, N. Skidmore⁵⁶, R. Skuza¹⁷,
T. Skwarnicki⁶², M. W. Slater⁴⁷, J. C. Smallwood⁵⁷, J. G. Smeaton⁴⁹, E. Smith⁴⁴, K. Smith⁶¹, M. Smith⁵⁵,
A. Snoch³², L. Soares Lavra⁹, M. D. Sokoloff⁵⁹, F. J. P. Soler⁵³, A. Solomin^{38,48}, A. Solovev³⁸, I. Solovyev³⁸,
R. Song⁶³, F. L. Souza De Almeida², B. Souza De Paula², B. Spaan,^{15,a} E. Spadaro Norella^{25,p}, E. Spedicato²⁰,
E. Spiridenkov,³⁸ P. Spradlin⁵³, V. Sriskaran⁴², F. Stagni⁴², M. Stahl⁴², S. Stahl⁴², S. Stanislaus⁵⁷, E. N. Stein⁴²,
O. Steinkamp⁴⁴, O. Stenyakin,³⁸ H. Stevens¹⁵, S. Stone^{62,a}, D. Strelakina³⁸, Y. S. Su⁶, F. Suljik⁵⁷, J. Sun²⁷,
L. Sun⁶⁸, Y. Sun⁶⁰, P. Svihra⁵⁶, P. N. Swallow⁴⁷, K. Swientek³⁴, A. Szabelski³⁶, T. Szumlak³⁴,
M. Szymanski⁴², Y. Tan³, S. Taneja⁵⁶, A. R. Tanner,⁴⁸ M. D. Tat⁵⁷, A. Terentev³⁸, F. Teubert⁴², E. Thomas⁴²,
D. J. D. Thompson⁴⁷, K. A. Thomson⁵⁴, H. Tilquin⁵⁵, V. Tisserand⁹, S. T'Jampens⁸, M. Tobin⁴,
L. Tomassetti^{21,d}, G. Tonani^{25,p}, X. Tong⁵, D. Torres Machado¹, D. Y. Tou³, S. M. Trilov⁴⁸, C. Trippl⁴³,
G. Tuci⁶, A. Tully⁴³, N. Tuning³², A. Ukleja³⁶, D. J. Unverzagt¹⁷, A. Usachov³², A. Ustyuzhanin³⁸,
U. Uwer¹⁷, A. Vagner³⁸, V. Vagnoni²⁰, A. Valassi⁴², G. Valenti²⁰, N. Valls Canudas⁷⁶, M. van Beuzekom³²,
M. Van Dijk⁴³, H. Van Hecke⁶¹, E. van Herwijnen⁵⁵, C. B. Van Hulse^{40,v}, M. van Veghel⁷³, R. Vazquez Gomez³⁹,
P. Vazquez Regueiro⁴⁰, C. Vázquez Sierra⁴², S. Vecchi²¹, J. J. Velthuis⁴⁸, M. Veltri^{22,w}, A. Venkateswaran⁴³,
M. Veronesi³², M. Vesterinen⁵⁰, D. Vieira⁵⁹, M. Vieites Diaz⁴³, X. Vilasis-Cardona⁷⁶, E. Vilella Figueras⁵⁴,
A. Villa²⁰, P. Vincent¹³, F. C. Volle¹¹, D. vom Bruch¹⁰, A. Vorobyev,³⁸ V. Vorobyev,³⁸ N. Voropaev³⁸, K. Vos⁷⁴,
C. Vrahas⁵², R. Waldi¹⁷, J. Walsh²⁹, G. Wan⁵, C. Wang¹⁷, G. Wang⁷, J. Wang⁵, J. Wang⁴, J. Wang³,
J. Wang⁶⁸, M. Wang⁵, R. Wang⁴⁸, X. Wang⁶⁶, Y. Wang⁷, Z. Wang⁴⁴, Z. Wang³, Z. Wang⁶, J. A. Ward^{50,63},
N. K. Watson⁴⁷, D. Websdale⁵⁵, Y. Wei⁵, C. Weisser,⁵⁸ B. D. C. Westhenry⁴⁸, D. J. White⁵⁶, M. Whitehead⁵³,
A. R. Wiederhold⁵⁰, D. Wiedner¹⁵, G. Wilkinson⁵⁷, M. K. Wilkinson⁵⁹, I. Williams⁴⁹, M. Williams⁵⁸,
M. R. J. Williams⁵², R. Williams⁴⁹, F. F. Wilson⁵¹, W. Wislicki³⁶, M. Witek³⁵, L. Witola¹⁷, C. P. Wong⁶¹,
G. Wormser¹¹, S. A. Wotton⁴⁹, H. Wu⁶², J. Wu⁷, K. Wyllie⁴², Z. Xiang⁶, D. Xiao⁷, Y. Xie⁷, A. Xu⁵, J. Xu⁶,
L. Xu³, L. Xu³, M. Xu⁵⁰, Q. Xu⁶, Z. Xu⁹, Z. Xu⁶, D. Yang³, S. Yang⁶, X. Yang⁵, Y. Yang⁶, Z. Yang⁵,
Z. Yang⁶⁰, L. E. Yeomans⁵⁴, V. Yeroshenko¹¹, H. Yeung⁵⁶, H. Yin⁷, J. Yu⁶⁵, X. Yuan⁶², E. Zaffaroni⁴³,
M. Zavertyaev¹⁶, M. Zdybal³⁵, O. Zenaiev⁴², M. Zeng³, C. Zhang⁵, D. Zhang⁷, L. Zhang³, S. Zhang⁶⁵,
S. Zhang⁵, Y. Zhang⁵, Y. Zhang⁵⁷, A. Zharkova³⁸, A. Zhelezov¹⁷, Y. Zheng⁶, T. Zhou⁵, X. Zhou⁶, Y. Zhou⁶,
V. Zhovkovska¹¹, X. Zhu³, X. Zhu⁷, Z. Zhu⁶, V. Zhukov^{14,38}, Q. Zou^{4,6}, S. Zucchelli^{20,f},
D. Zuliani²⁸ and G. Zunica⁵⁶

(LHCb Collaboration)

- ¹Centro Brasileiro de Pesquisas Físicas (CBPF), Rio de Janeiro, Brazil
²Universidade Federal do Rio de Janeiro (UFRJ), Rio de Janeiro, Brazil
³Center for High Energy Physics, Tsinghua University, Beijing, China
⁴Institute of High Energy Physics (IHEP), Beijing, China
⁵School of Physics State Key Laboratory of Nuclear Physics and Technology, Peking University, Beijing, China
⁶University of Chinese Academy of Sciences, Beijing, China
⁷Institute of Particle Physics, Central China Normal University, Wuhan, Hubei, China
⁸Université Savoie Mont Blanc, CNRS, IN2P3-LAPP, Annecy, France
⁹Université Clermont Auvergne, CNRS/IN2P3, LPC, Clermont-Ferrand, France
¹⁰Aix Marseille Université, CNRS/IN2P3, CPPM, Marseille, France
¹¹Université Paris-Saclay, CNRS/IN2P3, IJCLab, Orsay, France
¹²Laboratoire Leprince-Ringuet, CNRS/IN2P3, Ecole Polytechnique, Institut Polytechnique de Paris, Palaiseau, France
¹³LPNHE, Sorbonne Université, Paris Diderot Sorbonne Paris Cité, CNRS/IN2P3, Paris, France
¹⁴I. Physikalisches Institut, RWTH Aachen University, Aachen, Germany
¹⁵Fakultät Physik, Technische Universität Dortmund, Dortmund, Germany
¹⁶Max-Planck-Institut für Kernphysik (MPIK), Heidelberg, Germany
¹⁷Physikalisches Institut, Ruprecht-Karls-Universität Heidelberg, Heidelberg, Germany
¹⁸School of Physics, University College Dublin, Dublin, Ireland
¹⁹INFN Sezione di Bari, Bari, Italy
²⁰INFN Sezione di Bologna, Bologna, Italy
²¹INFN Sezione di Ferrara, Ferrara, Italy
²²INFN Sezione di Firenze, Firenze, Italy
²³INFN Laboratori Nazionali di Frascati, Frascati, Italy
²⁴INFN Sezione di Genova, Genova, Italy
²⁵INFN Sezione di Milano, Milano, Italy
²⁶INFN Sezione di Milano-Bicocca, Milano, Italy
²⁷INFN Sezione di Cagliari, Monserrato, Italy
²⁸Università degli Studi di Padova, Università e INFN, Padova, Padova, Italy
²⁹INFN Sezione di Pisa, Pisa, Italy
³⁰INFN Sezione di Roma La Sapienza, Roma, Italy
³¹INFN Sezione di Roma Tor Vergata, Roma, Italy
³²Nikhef National Institute for Subatomic Physics, Amsterdam, Netherlands
³³Nikhef National Institute for Subatomic Physics and VU University Amsterdam, Amsterdam, Netherlands
³⁴AGH—University of Science and Technology, Faculty of Physics and Applied Computer Science, Kraków, Poland
³⁵Henryk Niewodniczanski Institute of Nuclear Physics Polish Academy of Sciences, Kraków, Poland
³⁶National Center for Nuclear Research (NCBJ), Warsaw, Poland
³⁷Horia Hulubei National Institute of Physics and Nuclear Engineering, Bucharest-Magurele, Romania
³⁸Affiliated with an institute covered by a cooperation agreement with CERN
³⁹ICCUB, Universitat de Barcelona, Barcelona, Spain
⁴⁰Instituto Galego de Física de Altas Enerxías (IGFAE), Universidade de Santiago de Compostela, Santiago de Compostela, Spain
⁴¹Instituto de Física Corpuscular, Centro Mixto Universidad de Valencia—CSIC, Valencia, Spain
⁴²European Organization for Nuclear Research (CERN), Geneva, Switzerland
⁴³Institute of Physics, Ecole Polytechnique Fédérale de Lausanne (EPFL), Lausanne, Switzerland
⁴⁴Physik-Institut, Universität Zürich, Zürich, Switzerland
⁴⁵NSC Kharkiv Institute of Physics and Technology (NSC KIPT), Kharkiv, Ukraine
⁴⁶Institute for Nuclear Research of the National Academy of Sciences (KINR), Kyiv, Ukraine
⁴⁷University of Birmingham, Birmingham, United Kingdom
⁴⁸H.H. Wills Physics Laboratory, University of Bristol, Bristol, United Kingdom
⁴⁹Cavendish Laboratory, University of Cambridge, Cambridge, United Kingdom
⁵⁰Department of Physics, University of Warwick, Coventry, United Kingdom
⁵¹STFC Rutherford Appleton Laboratory, Didcot, United Kingdom
⁵²School of Physics and Astronomy, University of Edinburgh, Edinburgh, United Kingdom
⁵³School of Physics and Astronomy, University of Glasgow, Glasgow, United Kingdom
⁵⁴Oliver Lodge Laboratory, University of Liverpool, Liverpool, United Kingdom

- ⁵⁵*Imperial College London, London, United Kingdom*
- ⁵⁶*Department of Physics and Astronomy, University of Manchester, Manchester, United Kingdom*
- ⁵⁷*Department of Physics, University of Oxford, Oxford, United Kingdom*
- ⁵⁸*Massachusetts Institute of Technology, Cambridge, Massachusetts, USA*
- ⁵⁹*University of Cincinnati, Cincinnati, Ohio, USA*
- ⁶⁰*University of Maryland, College Park, Maryland, USA*
- ⁶¹*Los Alamos National Laboratory (LANL), Los Alamos, New Mexico, USA*
- ⁶²*Syracuse University, Syracuse, New York, USA*
- ⁶³*School of Physics and Astronomy, Monash University, Melbourne, Australia*
(associated with Department of Physics, University of Warwick, Coventry, United Kingdom)
- ⁶⁴*Pontifícia Universidade Católica do Rio de Janeiro (PUC-Rio), Rio de Janeiro, Brazil*
(associated with Universidade Federal do Rio de Janeiro (UFRJ), Rio de Janeiro, Brazil)
- ⁶⁵*Physics and Micro Electronic College, Hunan University, Changsha City, China*
(associated with Institute of Particle Physics, Central China Normal University, Wuhan, Hubei, China)
- ⁶⁶*Guangdong Provincial Key Laboratory of Nuclear Science, Guangdong-Hong Kong Joint Laboratory of Quantum Matter, Institute of Quantum Matter, South China Normal University, Guangzhou, China*
(associated with Center for High Energy Physics, Tsinghua University, Beijing, China)
- ⁶⁷*Lanzhou University, Lanzhou, China (associated with Institute of High Energy Physics (IHEP), Beijing, China)*
- ⁶⁸*School of Physics and Technology, Wuhan University, Wuhan, China*
(associated with Center for High Energy Physics, Tsinghua University, Beijing, China)
- ⁶⁹*Departamento de Física, Universidad Nacional de Colombia, Bogota, Colombia*
(associated with LPNHE, Sorbonne Université, Paris Diderot Sorbonne Paris Cité, CNRS/IN2P3, Paris, France)
- ⁷⁰*Universität Bonn—Helmholtz-Institut für Strahlen und Kernphysik, Bonn, Germany*
(associated with Physikalisches Institut, Ruprecht-Karls-Universität Heidelberg, Heidelberg, Germany)
- ⁷¹*Eotvos Lorand University, Budapest, Hungary (associated with European Organization for Nuclear Research (CERN), Geneva, Switzerland)*
- ⁷²*INFN Sezione di Perugia, Perugia, Italy (associated with INFN Sezione di Ferrara, Ferrara, Italy)*
- ⁷³*Van Swinderen Institute, University of Groningen, Groningen, Netherlands*
(associated with Nikhef National Institute for Subatomic Physics, Amsterdam, Netherlands)
- ⁷⁴*Universiteit Maastricht, Maastricht, Netherlands*
(associated with Nikhef National Institute for Subatomic Physics, Amsterdam, Netherlands)
- ⁷⁵*Tadeusz Kosciuszko Cracow University of Technology, Cracow, Poland*
(associated with Henryk Niewodniczanski Institute of Nuclear Physics Polish Academy of Sciences, Kraków, Poland)
- ⁷⁶*DS4DS, La Salle, Universitat Ramon Llull, Barcelona, Spain*
(associated with ICCUB, Universitat de Barcelona, Barcelona, Spain)
- ⁷⁷*Department of Physics and Astronomy, Uppsala University, Uppsala, Sweden*
(associated with School of Physics and Astronomy, University of Glasgow, Glasgow, United Kingdom)
- ⁷⁸*University of Michigan, Ann Arbor, Michigan, USA*
(associated with Syracuse University, Syracuse, New York, USA)

^aDeceased.

^bAlso at Università di Firenze, Firenze, Italy.

^cAlso at Scuola Normale Superiore, Pisa, Italy.

^dAlso at Università di Ferrara, Ferrara, Italy.

^eAlso at Università di Milano Bicocca, Milano, Italy.

^fAlso at Università di Bologna, Bologna, Italy.

^gAlso at Università di Genova, Genova, Italy.

^hAlso at Universidad Nacional Autónoma de Honduras, Tegucigalpa, Honduras.

ⁱAlso at Università di Bari, Bari, Italy.

^jAlso at Università di Cagliari, Cagliari, Italy.

^kAlso at Università di Perugia, Perugia, Italy.

^lAlso at Università di Roma Tor Vergata, Roma, Italy.

^mAlso at Universidade de Brasília, Brasília, Brazil.

ⁿAlso at Hangzhou Institute for Advanced Study, UCAS, Hangzhou, China.

^oAlso at Università di Siena, Siena, Italy.

^pAlso at Università degli Studi di Milano, Milano, Italy.

^qAlso at Central South University, Changsha, China.

^rAlso at Università di Padova, Padova, Italy.

^sAlso at Excellence Cluster ORIGINS, Munich, Germany.

^tAlso at Università di Pisa, Pisa, Italy.

^uAlso at Università della Basilicata, Potenza, Italy.

^vAlso at Universidad de Alcalá, Alcalá de Henares, Spain.

^wAlso at Università di Urbino, Urbino, Italy.